Molecular Science

AIMS Molecular Science, 11(3): 231–250.
DOI: 10.3934/molsci.2024014
Received: 18 December 2023
Revised: 01 June 2024
Accepted: 28 June 2024
Published: 10 July 2024

http://www.aimspress.com/journal/Molecular

Research article

Loading diltiazem onto surface-modified nanostructured lipid carriers to evaluate its apoptotic, cytotoxic, and inflammatory effects on human breast cancer cells

Vahid Pouresmaeil[1,*], Marwa Mawlood Salman Al-zand[2], Aida Pouresmaeil[3], Seyedeh Samira Saghravanian[3] and Masoud Homayouni Tabrizi[3]

[1] Department of Biochemistry, Faculty of Medicine, Mashhad Medical Sciences, Islamic Azad University, Mashhad, Iran
[2] Department of Biology, Science and Research Branch, Islamic Azad University, Tehran, Iran
[3] Department of Biology, Mashhad Branch, Islamic Azad University, Mashhad, Iran

* **Correspondence:** Email: vahidpouresmail@yahoo.fr, pouresmaeil.v@iaumshms.ac.ir; Tel: +985132250049; Fax: +985132250048.

Abstract: The main goal of cancer treatment is to ensure that the drug reaches the tumor tissue and to reduce the side effects of the drug. This study was conducted to synthesize a novel nanostructured lipid carrier modified with chitosan-folate to deliver diltiazem to cancer cell lines and to evaluate its anticancer effect. Dynamic light scattering (DLS), field emission scanning electron microscopy (FESEM), and Fourier transform infrared spectrometer (FTIR) methods were used to characterize the nanoparticles. The cytotoxicity effect on cancer cell lines variants was measured. Flow cytometry was used for cell cycle analysis, and reverse transcription polymerase chain reaction (RT-PCR) was performed to assess the induction of apoptosis. The inflammatory effects were evaluated by molecular analysis, and the 2,2'-azino-bis(3-ethylbenzothiazoline-6-sulfonic acid, 2,2-Diphenyl-1-picrylhydrazyl, and Ferric reducing antioxidant power methods were used to measure the antioxidant power of the nanoparticles. The results reported the mean of the real and hydrodynamic diameter of the nanoparticles as 87.7 and 249 nm, respectively, and the encapsulation efficiency of diltiazem was reported to be 86.6%. The cytotoxicity results revealed that the breast cancer cells were more sensitive to treatment, with a median concentration of 33.5µg/ml. Additionally, the nanoparticle treatment led to the arrest of cells in the SubG1 phase while increasing the expression of caspases 3 and 9, which indicates the activation of the internal pathway of apoptosis. Additionally, the increase in the

expression of interleukins 6 and 10 suggests an effect of the nanoparticles on inflammation. In addition, the ability to inhibit 2,2'-azino-bis (3-ethylbenzothiazoline-6-sulfonic acid and 2,2-Diphenyl-1-picrylhydrazyl free radicals with an average concentration of 577, which is more significant than 1000 µg/ml, and the ability of the nanoparticles to reduce iron ions confirmed the antioxidant effect of diltiazem-loaded nanostructured lipid carriers. These results suggest that the nanoparticles have an excellent potential to treat breast cancer.
Keywords: diltiazem; nanostructured lipid carriers; anti-inflammatory effect; apoptosis; breast cancer cells

Abbreviations: Nanostructured lipid carriers (NLC); Diltiazem (DIL); Dynamic Light Scattering (DLS); Field emission scanning electron microscope (FESEM); Fourier transform infrared (FTIR); 3-(4,5-dimethylthiazol-2-yl)-2,5-diphenyltetrazolium bromide (MTT); Acridine orange *(*AO*)* ; DAPI or Propidium iodide (PI); *Real-time* polymerase chain reaction (RTqPCT); 2,2-azinobis (3-ethylbenzothiazoline-6-sulfonic acid) (ABTS) ; 2,2-diphenyl-1-picrylhydrazyl (DPPH); Polydispersity Index (PDI); 1-Ethyl-3-(3-dimethylaminopropyl) carbodiimide (EDC); N-Hydroxysuccinimide (NHS); Breast cancer cell lines (MCF-7); (MDA-MB231); Gastric cancer cell lines (AGS); Colon cancer cell lines (HT-29); Human dermal fibroblasts (HDF).

1. Introduction

The sizes of nanoparticles (NPs) vary from 10 to 500 nm with the various compounds [1]. These particles have been extensively studied for their properties and used in biomolecular fields such as drug delivery and cancer therapy [2]. When nanoparticles are used in biomedical applications, two essential properties, namely toxicity and cellular uptake, must be considered. In reality, the biocompatibility of nanoparticles is crucial for their suitability for biomedical purposes [3], and the ability of NPs to penetrate the target cells compared to non-target cells is essential [4]. Modifying NPs with ligands that have a specific affinity for these markers could improve the identification of desired compounds for the target cells [5]. Nanostructured lipid carriers (NLCs) were developed as the second generation of lipid NPs to overcome the shortcomings of the first generation, solid lipid NPs (SLNs). Environmentally friendly lipids are used to prepare NLCs. In addition, NLCs protect the loaded drug, increase the half-life and bioavailability, and reduce the need for high drug doses [6,7].

Chitosan (CS) is a linear polysaccharide composed of β-D-glucosamine and N-acetyl-D-glucosamine; therefore, it produces a minimal immune response and has biocompatibility and biodegradability properties. Applying chitosan on the surface of the NPs could increase the penetration of the nanocarrier due to its ability to open tight junctions of the epithelium. Chitosan has mucosal adhesion properties, so its use in drug delivery through the digestive system can be beneficial. In addition, chitosan's positive charge allows it to connect to negatively charged cells by either ionic or hydrogen bonding and hydrophobic interactions, increasing its ability to deliver drugs to cancer cells [8,9].

Folate is one of the target biomolecules of cancer cells with overexpressed receptors which prevents the strong membrane barrier of tumors with weak vessels [10]. The folate receptor (FR) is overexpressed in various human cancers, including breast, ovary, kidney, and lung. Therefore, it's considered a tumor-specific target platform [11].

Diltiazem (DIL) is a non-dihydropyridine antihypertensive drug and an L-type voltage-dependent

calcium channel blocker (CCB). DIL is primarily known as a calcium channel blocker, and is commonly used to treat high blood pressure, angina, and certain abnormal heart rhythms. While its primary function is in cardiovascular therapy, some studies have suggested that it may exhibit an anti-tumor activity. The anti-tumor mechanism of DIL is not yet fully understood, but research has pointed to several possible pathways:

1) Inhibition of tumor cell proliferation by interfering with their cell division processes [12].
2) Induction of apoptosis [13].
3) Inhibition of angiogenesis and metastasis by mediating growth differentiation factor 15 and the epithelial-mesenchymal transition [14].
4) Modulation of calcium signaling plays a crucial role in cellular processes, including cell growth and survival. As a calcium channel blocker, DIL may affect these processes in cancer cells by altering calcium signaling [15].

It is essential to note that these findings are from preclinical studies and more research is needed to fully understand DIL's anti-tumor activity and its potential as an anti-cancer agent. In this regard, several studies have demonstrated the antitumor effects of specific CCBs on cancers, through mechanisms such as the induction of autophagy and apoptosis, the inhibition of cancer growth, and the reversal of resistance to chemotherapy by the inhibition of multidrug resistance proteins [15,16].

Caspase 9 and Caspase 3, as well as interleukins (IL-6 and IL-10), serve as biomarkers for apoptotic cell death and inflammation, respectively [17–20]. Measuring the expression levels of these genes can function as an indicator for apoptotic death and inflammation. The survival and metastatic capabilities of cancer cells are intricately linked to their ability to inhibit apoptotic cell death and stimulate inflammatory responses. These strategies have been targeted in breast cancer cells to inhibit their proliferation and to modulate inflammatory processes. Furthermore, understanding the molecular mechanisms underlying these strategies can provide valuable insights into potential therapeutic targets. By modulating the expression and activity of caspases and interleukins, researchers aim to enhance the effectiveness of existing cancer treatments and develop novel therapeutic approaches. This knowledge can contribute to the design of personalized medicine strategies, tailoring treatments to individual patients based on their unique molecular profiles and disease characteristics. Ultimately, this may lead to improved patient outcomes and a better understanding of cancer biology [21–23].

In this research, NLC nanoparticles were synthesized, DIL was loaded into the NLC, the surface of the nanoparticle was coated with a layer of chitosan-conjugated folate (DIL-CF-NLC), and after nanoparticles characterization, its anticancer effects on various cancer cell lines were evaluated.

2. Materials and methods

2.1. DIL-NLC synthetizing

Homogenization and ultra-sonication techniques were used for this synthesis [24]. To prepare the lipid matrix, oleic acid (a liquid lipid), glyceryl monostearate (a solid lipid), and lecithin were combined. Subsequently, the medication was incorporated into the lipid matrix and incubated at 80 ℃ until it melted. The aqueous phase was prepared by dissolving Tween 80 in 20 mL of purified water (DW) and then incubated at 80 ℃. Finally, the liquid phase was rapidly added to the lipid phase, the resulting mixture was homogenized, and subsequently subjected to sonication.

2.2. DIL-NLC Characterisation

The average size, dispersion, and zeta potential of the synthesized nanoparticles were measured in triplicate by the dynamic light scattering (DLS) method as in previous studies [25,26].

2.3. Surface modification of nanoparticles

To bind folic acid (FA) to CS, a solution of FA-N-Hydroxysuccinimide (NHS) was added dropwise to the CS dissolved in acetic acid and then incubated for 24 hours; finally, it was precipitated by centrifugation for dialysis and lyophilization. To immobilize FA-CS on the surface of the nanoparticles, the FA-CS powder was dissolved in acetic acid (1%). Then, the CF solution was slowly added to the solution containing the NPS. After centrifugation, the obtained precipitate was lyophilized.

2.4. DIL-CF-NLC Characterisation

The average size, dispersion, and surface charge of the synthesized DIL-CF-NLC were measured as mentioned above. Field emission scanning electron microscopy (FESEM) was used to examine the morphology of the sample along with the particle size, and Fourier transform infrared spectroscopy (FTIR) was used to identify the organic and polymeric materials. These techniques were carried out as previously described [25,26].

2.5. Encapsulation of DIL in CFN-NPs

Initially, serial DIL concentrations were prepared, their absorbance was measured at 226 nm, and its standard plot was drawn. Then, the absorbance of the supernatant obtained from the synthesis was also measured at the same wavelength, and the amount of free drug in the supernatant was calculated by including the resulting number in the calibration curve formula. Finally, the amount of encapsulated drug was calculated by subtracting the amount of free drug from the total amount of drug.

2.6. Cytotoxicity effects of DIL in CFN-NPs

All the cell lines, including Breast cancer cell lines (MCF-7 and MDA-MB231), Gastric cancer cell lines (AGS), Colon cancer cell lines (HT-29), and Human dermal fibroblasts (HDF), were provided from the Pasteur Institute of Iran. The given cell cultures were initially seeded at a density of 6×10^4 cells per square centimeter and maintained in Dulbecco's Modified Eagle Medium (DMEM) from Gibco, supplemented with 10% fetal bovine serum (FBS), and antibiotics including 100 units per milliliter of penicillin and 100 milligrams per milliliter of streptomycin. They were kept under standard conditions, namely a temperature of 37 ℃, 95% humidity, and a 5% carbon dioxide (CO_2) atmosphere. 6×10^4 cells were added to each well of a 96-well plate and incubated for another 24 hours under the same specified conditions. In this experiment, cultured cells were exposed to varying concentrations of FCPS-NPs (15.6, 31.2, 62.5, and 125 μg/mL). Following a 48-hour incubation period, the medium was replaced with fresh media containing MTT (0.5 mg/mL). After 3 hours, a DMSO solution was added to each well to dissolve the formed formazan. The resulting formazan concentration was determined by measuring the absorbance at 570 nm using a Stat Fax 2100 plate reader. The cell survival

rate was calculated using the provided equation:

$$\%CV = (\text{Absorbance of control}/\text{Absorbance of the sample}) \times 100.$$

2.7. Apoptosis Induction by DIL-CAN-NPs

2.7.1. Cycle cell investigation

The cells were cultured for 24 hours; at that point, the culture medium was depleted and supplanted with the treatment medium containing the concentrations obtained by the MTT method. After washing, 1 mL of trypsin was added to each well; at that point, the cells were isolated from the foot of the plate, and 1 mL of culture medium was added to each well. After centrifugation, the supernatant was depleted and 300 μL of PI color was included in the cell pellet and analyzed by the flow cytometry method.

2.7.2. Evaluation of apoptosis and inflammatory genes by real-time PCR

For this purpose, MCF7 cells were cultured and treated with variant concentrations of nanoparticles. After 48 h, RNA from the cells was isolated. After their quantification by nanodrop, the resulting RNA was used as a template for cDNA synthesis. Finally, the reaction mixture was prepared with cDNA, specific primers, and Cyber Green, and each gene's expression was analyzed using the PCR method (Table 1).

Table 1. The primer sequence of target genes.

Gene	Forward	Reverse
GAPDH	GCAGGGGGGAGCCAAAAGGGT	TGGGTGCCAGTGATGGCATGG
Caspase 3	CTGGACTGTGGCATTGAGAC	ACAAAGCGACTGGATGAACC
Caspase 9	CCAGAGATTCGCAAACCAGAGG	GAGCACCGACATCACCAAATCC
Il-6	CAAATTCGGTACATCCTC	CTGGCTTGTTCCTCACTA
Il-10	TGGAGGACTTTAAGGGTTAC	GATGTCTGGGTCTTGGTT

2.8. Anti-oxidant ability of DIL-CAN-NPs

To assess the antioxidant capacity of the NPs, serial concentrations of the nanoparticles were prepared; then, an equal amount of 2,2-azinobis (3-ethylbenzothiazoline-6-sulfonic acid) (ABTS) free radical (or 2,2-diphenyl-1-picrylhydrazyl (DPPH) free radical) was added to each well. After 30 min of incubation at room temperature, the absorbance of the plates was analyzed at 734 nm. By substituting the results into the following formula, the percentage of ABTS free radical (or DPPH free radical) inhibition in the presence of the NPs was calculated:

$$\text{Inhibition percentage (\%)} = (\text{absorbance of control} - \text{absorbance of sample}/\text{absorbance of control}) \times 100$$

Additionally, the fluorescence recovery after photobleaching (FRAP) method was used to evaluate the ability of the NPs to reduce the iron ions (Fe^{3+}) [27].

2.9. Molecular docking analysis for diltiazem interactions with caspase 9, caspase 3, interleukin 6, and interleukin 10

Molecular processing involved using Windows 11 PCs equipped with Intel Core i7 1165G7 processors and NVidia GeForce MX450 graphics cards. The powerful Molecular Operating Environment (MOE) 2019 software was employed to prepare the ligands and for precise molecular docking [28].

2.9.1. Structure preparation of diltiazem and proteins

The initial step to prepare the DIL involved retrieving its three-dimensional configuration from databases. The compound was identified with the code 39186 in the PubChem database. Subsequently, it underwent energy optimization using a gradient of 0.001 Kcal/mol/A^2 within the MOE software and was saved in the MDB format.

To identify the protein configurations, we searched the Protein Data Bank (PDB) database and located the structures of caspase 9 (2AR9) [29], caspase 3 (1qx3) [30], interleukin-6 (1alu) [31], and interleukin-10 (2h24) [32]. Subsequently, these entities were obtained from the PDB site in the PDB form and imported into the MOE software. The removal of water and surplus ligands was performed for each compound.

2.9.2. Preparation of proteins for the molecular docking

The MOE QuickPrep feature was utilized to perform protonation and minimize the three-dimensional conformation of the proteins. Parameters including the AMBER10: EHT force field, “gas phase” solvation, and an RMS gradient of 0.001 kcal/mol/Å were applied to all protein structures. Protonated 3D configurations were chosen and flips for the asparagine (ASN)/glutamine (GLN)/histidine (HIS) residues were permitted.

2.9.3. Binding site prediction

Our search on the PDB site allowed us to identify the proteins, and we turned to the UniProtKB site for more detailed information regarding their structure and function. We located caspase 9 with code P55211, caspase 3 with code P42574, interleukin-6 with code P05231, and an interleukin-10 with code P22301. The active sites of caspase 9 contain the His237 and Ser287 amino acids, while those of caspase 3 contain the His121 and Cys163 amino acids. In the case of the interleukins, we analyzed their binding sites based on the Arg30, Arg182, Arg179, and Gln175 attached ligands for interleukin-6. Additionally, we identified the MOE funder site option in connection with interleukin-10. Furthermore, we utilized the MOE site finder option to pinpoint these amino acid-containing binding sites before creating dummy atoms for this region.

2.9.4. Docking process

In the MOE software, we selected dummy atoms to denote the target position within the Dock interface. Then, we imported the DIL combination in the MDB format and opted for the 'Rigid

Receptor' protocol along with 'Triangle Matcher/London dG' and 'Forcefield/GBVI-WSA dG' factors for placement and refinement. For docking, pose values of 30 and 5 were utilized. After completing the docking process, an assessment of the compound interactions was carried out through a ligand interaction analysis, as well as an evaluation of the scoring and binding energies. The S-score was utilized to assess the interactions, where lower S-score inhibitors exhibited strong interactions with proteins.

2.10. Statistical analysis

Data analysis was carried out by GraphPad Prism (V.8.0), and significant differences were considered at *P*-Value < 0.05. All the experiments were performed in triplicate. All data were expressed as mean (value ± SD).

3. Results

3.1. Nanoparticle size (dynamic light scattering technique)

The average diameter and hydrodynamic diameter of the lipid NPs were 62.56 and 214 nm, respectively, and the evaluation of the dispersion index showed the presence of monodisperse NPs, with a polydispersity index (PDI) of approximately 0.33, as seen in Figure 1A and B.

The average diameter and hydrodynamic diameter of the NPs were 87.7 and 249 nm, respectively, which shows a relatively larger size compared to NPs without chitosan-folate. This increase in the average diameter of the NPs can be attributed to the successful attachment of chitosan-folate. Examination of the dispersion index showed the presence of monodisperse particles with a PDI of 0.31, which shows a lower PDI compared to NPs without chitosan-folic acid, as seen in Figure 1C and D.

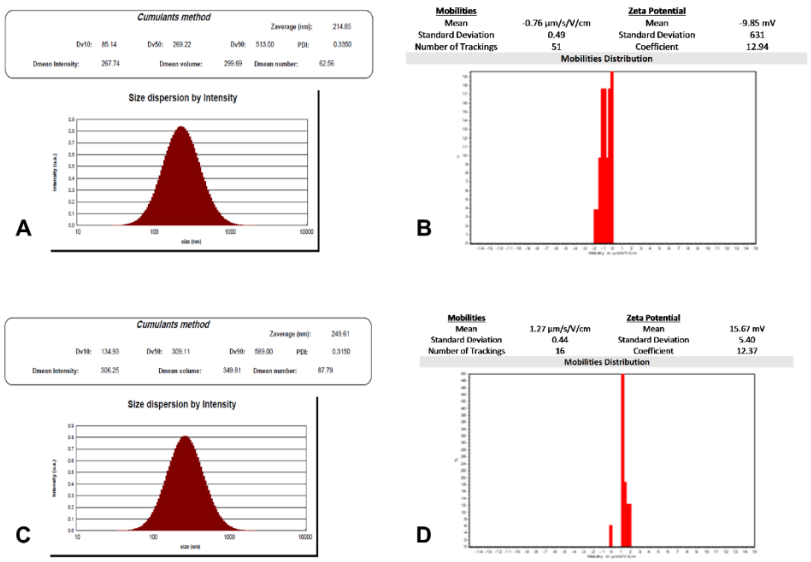

Figure 1. (A) Average size and dispersion index of DIL-NLC; (B) Evaluation of surface charge of DIL-NLC; (C) Size and dispersion index of DIL-CF-NLC; (D) Investigating the surface charge of DIL-CF-NLC.

3.2. Morphologic and chemical properties of nanoparticles by FESEM and FTIR methods

Examination of the morphology of the nanoparticles using an electron microscope (FESEM) showed spherical particles with a smooth surface and dimensions less than 100 nm. The distribution of the NP dispersion is uniform and without agglomerated parts, as seen in Figure 2A.

Figure 2B and D shows the FTIR spectrum of DIL-CF-NLC and NLCs. In the spectrum, a peak at 3306 cm^{-1} was recorded for the combined effect of the NH_2 and OH groups. The stretching peaks of CH_3/CH_2 appeared at 2920.09 and 2862 cm^{-1}, respectively [33]. The presence of a peak at 1733 cm^{-1} (C=O stretch) indicates that FA-CS is formed and CS successfully coats the NLC-NPs [34].

3.3. Drug encapsulation

The study of different concentrations of DIL was carried out at a wavelength of 226 nm, and the following standard curve was obtained with the formula Y = 0.309x + 0.0098 and the correlation coefficient of R^2 = 0.99. Placing the absorbance of the supernatant (0.412) in this formulation, the amount of free drug was 1.34 mg. These results showed that approximately 86.6% of DIL is encapsulated in nanoparticles, showing a high effectiveness, as seen in Figure 2C.

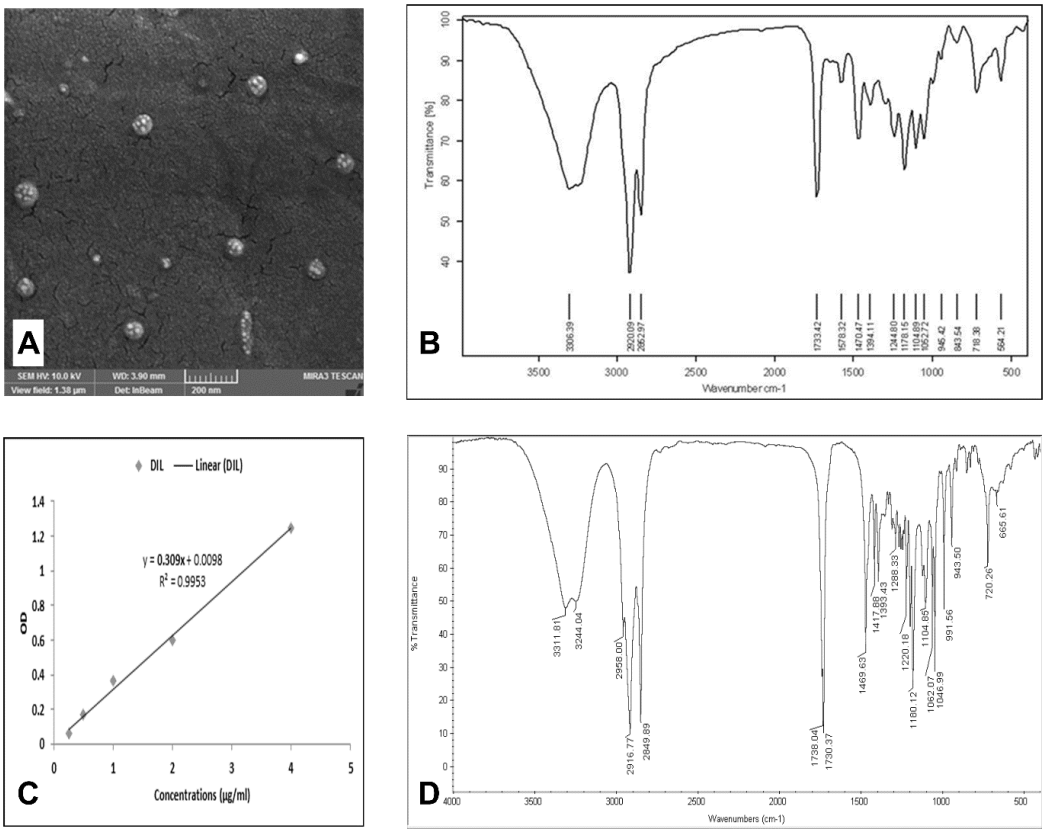

Figure 2. (A) Morphology of DIL-CFN-NLC using FESEM; (B) The FTIR spectrum of DIL-CF-NLC; (C) Drug (DIL) encapsulation: 86.6%; (D) The FTIR spectrum of NLCs.

3.4. Cytotoxicity effect of DIL-CF-NLC

The cytotoxicity of NPs on breast cancer cells (MCF-7) was studied by the MTT method; the results showed that NPs at a concentration of 33 µg/mL are capable of inhibiting 50% of the cancer cells (IC50). The increase in the inhibition rate with an increased concentration of NP treatment shows a concentration-dependent effect, as seen in Figure 3A.

The study demonstrated that the mean NP concentration that inhibited the breast cancer cells (MDA-MB231) was 108 µg/mL. At concentrations below 62 µg/mL, there was no substantial cytotoxicity observed against the cancerous cells. However, at a concentration of 125 µg/mL, 66% of the cells were suppressed by the NPs, as illustrated in Figure 3B.

The investigation on the gastric cancer cells (AGS) revealed that the NPs effectively inhibited 50% of the cancerous cell population when administered at a concentration of 65 µg/mL. In contrast, at a concentration below 30 µg/mL, the cell viability rate remained at 100%. However, at a concentration of 125 µg/mL, the growth of approximately 90% of the cells was significantly halted, as demonstrated in Figure 3C.

The study revealed that NPs exhibited a median toxicity against colon cancer cells (HT-29) at a concentration of around 105 µg/mL. The maximum inhibitory effect was observed at a concentration of 250 µg/mL, corresponding to approximately 73%, as depicted in Figure 3D.

As shown in Figure 3E, serving as a control, the assessment of NP toxicity against human dermal fibroblasts (HDF) demonstrated that the NPs did not exhibit any inhibitory influence on these cells at the examined concentrations. The results suggest a safe application of the NPs at concentrations below 250 µg/mL in clinical settings. Finally, given the results, the MCF-7 cells were found to be the most responsive to treatment and were selected for subsequent investigations.

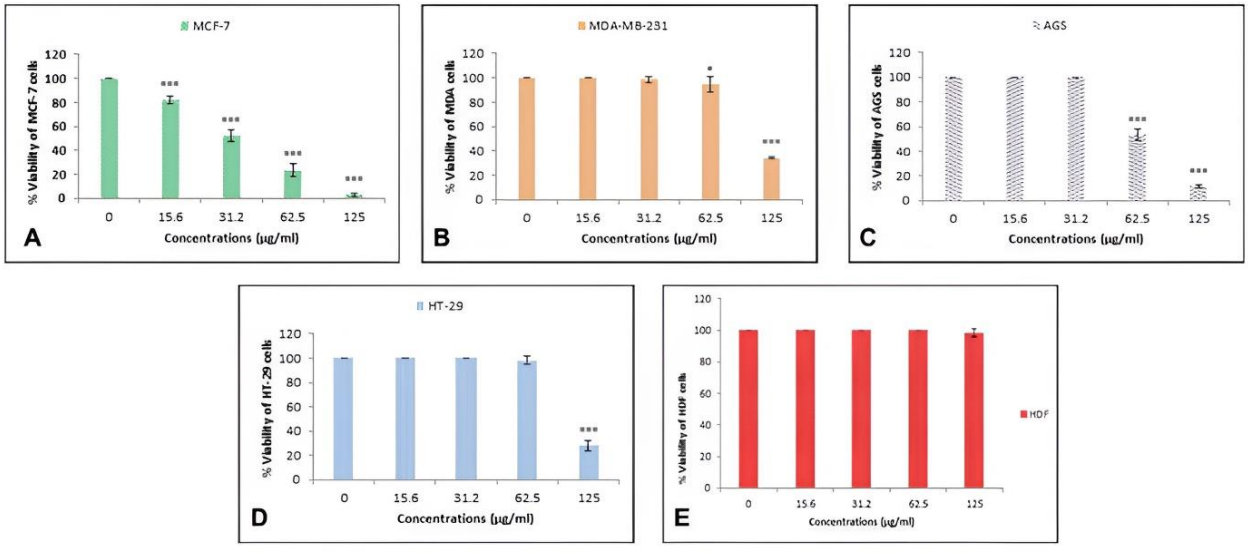

Figure 3. Cytotoxicity effect of DIL-CF-NLC on cancer cell lines. (A) Breast cancer cell lines (MCF-7); (B) Breast cancer cell lines MDA-MB231; (C) Gastric cancer cell lines (AGS); (D) Colon cancer cell lines (HT-29); (E) Human dermal fibroblasts (HDF) as control cells. The *, **, and *** indicate the P-values < 0.05, < 0.01, and < 0.001, respectively.

3.5. Apoptotic effect of DIL-CF-NLC

3.5.1. Flow Cytometry results

The cell cycle results show that the amount of SubG1, which indicates apoptotic cells, were 4.6, 22.1, 41.2, and 63.5%, respectively, compared to the different concentrations of NP treatments, as shown in Figure 4. The increase in the percentage of cells in this phase indicates cell cycle arrest under NP treatment. Additionally, cell cycle arrest in S and G2-M phases was observed in cells treated with a concentration of 15 µg/mL. These results show the cessation of cell growth after treatment with NPs and indicate the pro-apoptotic effects of the NPs.

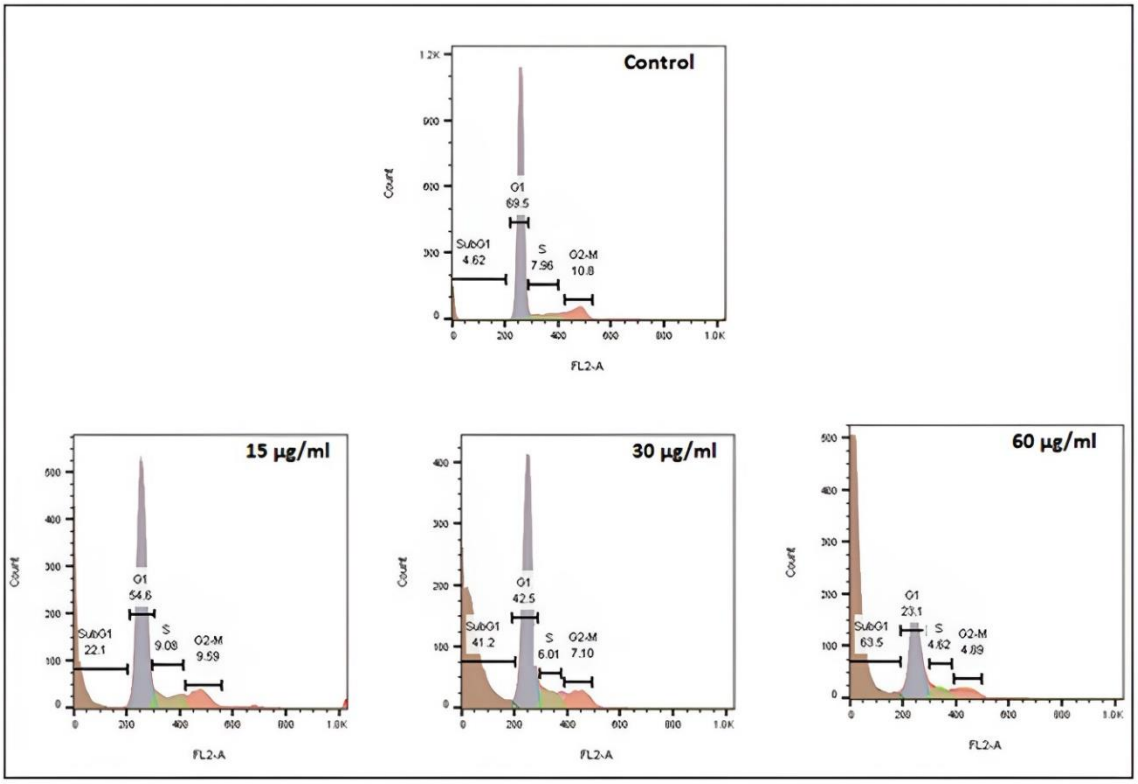

Figure 4. Apoptotic effect of DIL-CF-NLC: Cell cycle of cells treated with nanoparticles compared to control by flow cytometry method.

3.5.2. Molecular analysis

The results of caspase 9 gene expression, which is a gene involved in the mitochondrial pathway of apoptosis, showed an increase of caspase 9 expression in all cells treated with the NPs. This increase was significant in the cells treated with concentrations of 30 and 60 µg/mL, as shown in Figure 5A. These results show the activation of the intrinsic apoptosis pathway after treatment of cells with the NPs.

The Caspase 3 gene is activated as a common gene in both the intrinsic and extrinsic apoptosis pathways, and activation of both apoptosis pathways can change the expression of this gene. The

increased expression of this gene in the three concentrations studied indicates the activation of apoptosis in cells treated with the NPs, as shown in Figure 5B.

Interleukin-6 is a gene that promotes inflammation, and its effect on the inflammatory process depends on the pathways and factors involved. In this study, an increase in the expression of this gene was reported in the three concentrations studied; however, no significant increase in the expression of this gene was observed, as shown in Figure 5C.

The interleukin-10 gene is a gene that inhibits inflammation. The results showed an increase in the expression of this gene in all three treated groups; moreover, its expression only increased significantly in the group treated with a concentration of 60 µg/mL. These results show the anti-inflammatory effects of the NPs, as shown in Figure 5D.

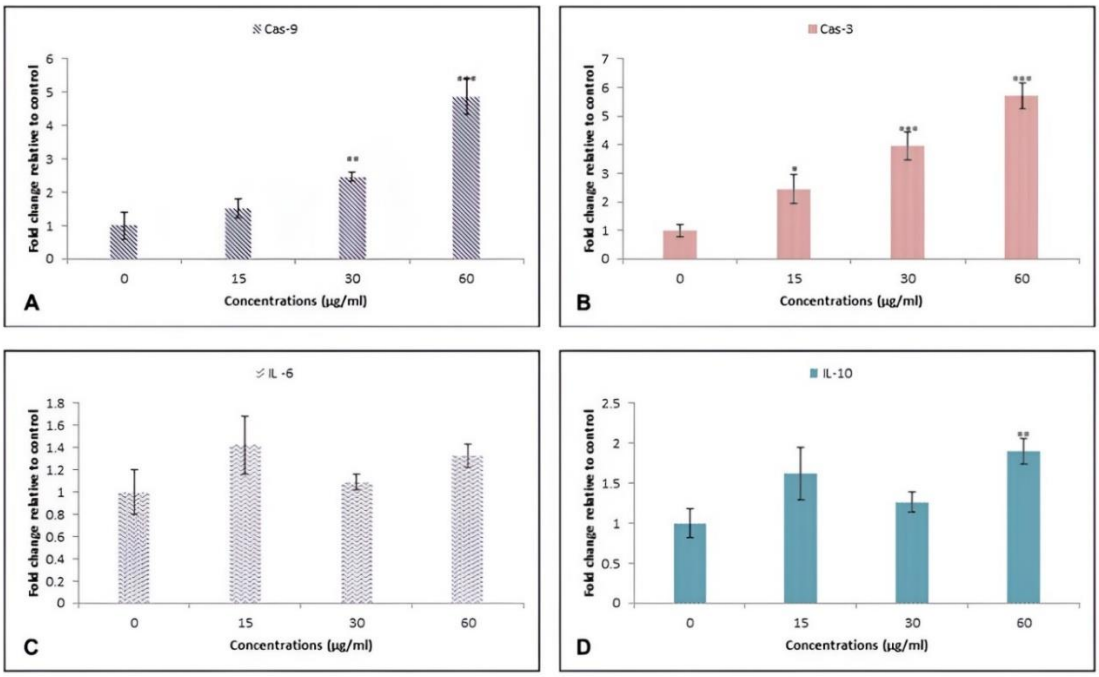

Figure 5. Molecular analysis: (A) Increased expression of Caspase 9 in cells treated with DIL-CF-NLC; (B) Increased expression of Caspase 3 in cells treated with DIL-CF-NLC; (C) Alteration of interleukin-6 expression in cells treated with DIL-CF-NLC; (D) Alteration of interleukin-10 expression in cells treated with DIL-CF-NLC. The *, **, and *** indicate the P-values < 0.05, < 0.01, and < 0.001, respectively.

3.6. Antioxidant ability of DIL-CF-NLC

The inhibitory effect of the NPs at different concentrations below 1 mg/mL on the ABTS free radicals was studied. The results showed that NPs at a concentration of 577 µg/mL are capable of inhibiting 50% of the ABTS free radicals. At concentrations below 250 µg/mL, the inhibition rate was less than 30%. These results show the dose-dependent inhibitory effects of the NPs on the ABTS free radicals, as shown in Figure 6A.

The study of DPPH free radical inhibition showed that the NPs had a moderate capacity to inhibit these radicals. The highest inhibitory effect (of approximately 25%) was reported at a concentration of

1000 µg, as shown in Figure 6B. These results show that the NPs are more effective at inhibiting the ABTS free radicals than the DPPH free radicals.

The Fe^{+2} reducing power was studied by the NPs using the FRAP method. The results showed that the NPs at a concentration of 2 mg/mL could reduce the iron ions by 0.18, as shown in Figures 6C and D. These results show the average antioxidant power of the NPs to reduce the iron ions.

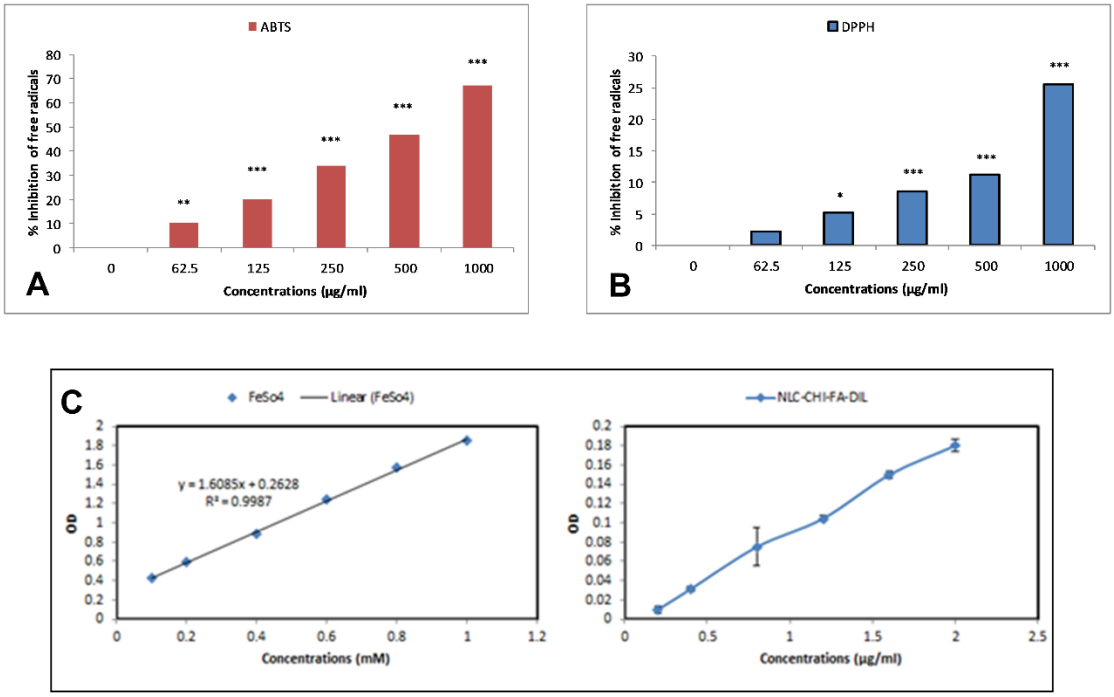

Figure 6. The antioxidant ability of DIL-CF-NLC: (A) Increase the rate of inhibition of ABTS free radicals exposed to DIL-CF-NLC; (B) Increase the rate of inhibition of DPPH free radicals exposed to DIL-CF-NLC; (C) Degree of inhibition of iron ions by DIL-CF-NLC (FRAP method). The *, **, and *** indicate the P-values < 0.05, < 0.01, and < 0.001, respectively.

3.7. Molecular docking results

The molecular docking findings were assessed following 300 placement positions for each protein (refer to Table 2). At the Caspase 9 active site, DIL formed bonds with Arg180 through the benzene ring and with Ser287 via C=O, resulting in an S-score of −6.71 (see Figure 7A).

For the active site within Caspase 3, DIL achieved an S-score of −5.99 by binding to amino acids His121, Cys163, and Thr166 (as depicted in Figure 7B). Additionally, at the interleukin-10 binding site, DIL established a bond with Asp25 through its S group and a bond via C=O to Arg104 while attaining an S-score of −6.54 (illustrated in Figure 7C), whereas at the interleukin-6 binding site showed an S-score of −5.62 by interacting with Arg182 and Arg179 (shown in Figure 7D).

Considering the results, DIL has the potential to impede the activity of these proteins. Based on the binding energy, DIL is more inclined towards caspase 9 than the other targets.

Table 2. S-score, as well as the energy of binding and the specific amino acids that are involved in the process of diltiazem binding to caspase 9, caspase 3, interleukin 10, and interleukin 6 proteins.

No	Complex protein-ligand	S-score	E-conformation	Amino Acids Bonds
1	Caspase 9-diltiazem	−6.71	−61.79	Arg180 and Ser287
2	Caspase 3-diltiazem	−5.99	−64.81	His121, Cys163, and Thr 166
3	Interleukin 10-diltiazem	−6.54	−69.11	Asp25 and Arg104
4	Interleukin 6-diltiazem	−5.62	−68.12	Arg182 and Arg179

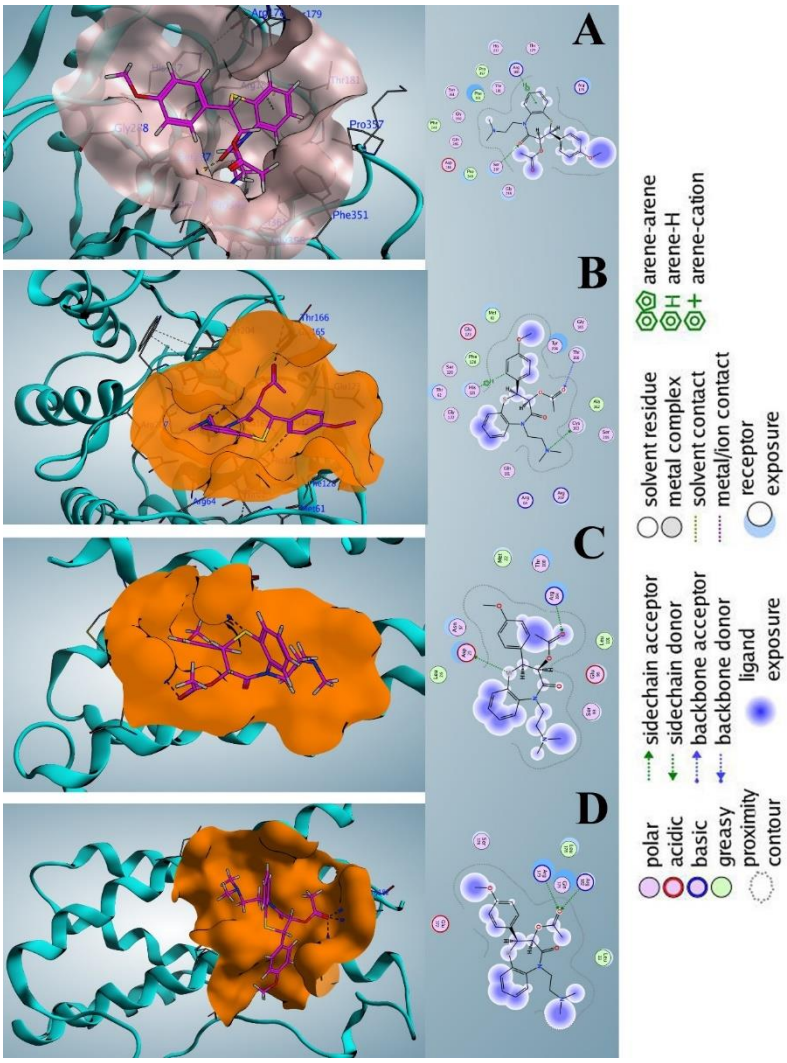

Figure 7. The diltiazem-protein interaction analysis. A) Caspase 9- diltiazem interaction, B) Caspase-3- diltiazem interaction, C) Interleukin 6- diltiazem interaction, D) Interleukin 10-diltiazem interaction. Most of the amino acids involved in these interactions are the key components of the protein's active site and significantly contribute to its function.

4. Discussion

To the best of our knowledge, this is the first study that encapsulates DIL into nanostructured lipid carriers coated with folate-conjugated CS to evaluate its anticancer activity against the human MCF-7

breast cancer cell line. The results exhibited the improved and selective toxicity of the DIL-CF-NLC.

The synthesized DIL-loaded NLC nanoparticles demonstrated an increase in size and a change in the surface charge from negative to positive after coating with folate-linked CS. These findings confirm the successful surface modification of the NPs. The drug encapsulation rate within the NPs was found to be 86%, indicating the effectiveness of the formulation method.

The results demonstrate that breast cancer cells are the most sensitive to treatment, with an average concentration of 33.5 μg/mL. The apoptosis process in breast cancer cells treated with NPs revealed that the cells were arrested at the SubG1 phase and exhibited increased gene expression for caspases 3 and 9. The anti-inflammatory effect of the NPs was confirmed by an increase in the expression of both the IL-10 and IL-6 genes. Additionally, the antioxidant effect of the NPs was confirmed through the inhibition of the ABTS and DPPH free radicals, with average concentrations of 577 and more significant than 1000 μg/mL, respectively.

Various drug delivery systems (DDS) types, such as proteins, liposomes, polymers, metals, and carbon nanocarriers, have become targets for cancer cell research [35]**.** Among them, NLCs are one of the best DDSs. These systems are often made of biodegradable and biocompatible materials based on a solid matrix, which increases drug loading while stabilizing and controlling the drug release in the digestive system [36]. Additionally, chitosan-based nanocarriers have enhanced cellular uptake of the NPs due to their biocompatibility, positive charge, suitable size and shape, hydrophilic nature, and interactions with specific cell surface receptors [37]. These factors collectively contribute to their efficient delivery into the target cells, making them a promising candidate for DDSs.

The compounds used in the formulation are effective due to their physicochemical properties, and the properties of the drug play an essential role in selecting the appropriate NLC nanoparticle synthesis technique. In this study, due to the nature of DIL, its ability to eliminate it by opsonizing the immune system, and the high efficiency of trapping bioactive compounds on liposome NPs, NLC nanocarriers were used to deliver this compound to the cancer cells.

Due to its increased permeation and retention efficiency, NLCs containing chemotherapeutic agents ranging in size from 30 nm to 100 nm are effectively removed by leaky vessels at tumor sites to transport drug cargo rapidly and less frequently than the more giant transporters cleared by the endothelial system in the liver and spleen [38].

Chemicals are bioactive compounds derived from plants that possess various therapeutic properties. Encapsulating these compounds within nanocarriers can enhance their solubility, stability, and bioavailability. In this regard, several synthetic and natural bioactive compounds have been encapsulated in different kinds of nano-drug delivery systems. For instance, Resveratrol-loaded solid lipid NPs showed an improved stability and enhanced permeability across Caco-2 cell monolayers compared to free resveratrol [39]. Additionally, Quercetin-loaded solid lipid NPs demonstrated a significant increase in the inhibition of human aldose reductase enzyme activity compared to free quercetin [40]. This enhanced inhibition can be attributed to quercetin's improved stability and solubility within the solid lipid NPs, which allows for a better interaction with the target enzyme and improved therapeutic potential in diabetes-related complications. Moreover, Curcumin-loaded polymeric NPs showed a 1.8-fold increase in the anti-inflammatory activity in lipopolysaccharide-activated RAW 264.7 macrophages compared to free curcumin. This enhanced activity can be attributed to the controlled release and prolonged circulation time of curcumin within the polymeric NPs, leading to a sustained anti-inflammatory response [41,42].

DIL, which is a calcium channel blocker, is commonly used to treat hypertension, angina, and

certain arrhythmias. Nano-drug delivery systems have gained significant attention in recent years due to their potential to enhance the therapeutic efficacy and to reduce the side effects of various drugs [43]. Herein, the folate-linked nanostructured lipid carriers encapsulated DIL and improved its selective cellular uptake.

This result indicates that encapsulation within solid lipid NPs can potentially increase the bioavailability of resveratrol, which may lead to improved therapeutic effects in various diseases.

The results of this study show that the synthesized NPs have an appropriate size for clinical applications and a low clearance rate from the reticuloendothelial system due to their small size. The loading of hydrophobic compounds into NLCs has been reported in various ways [7]. Some physical parameters, such as a spherical morphology, a uniform size distribution, and a surface charge above ±30 mV, are acceptable properties in terms of the stability and toxicity of NPs [44]. In the present study, due to the presence of FA on the surface of DIL-CF-NLC, cancer cells were studied more specifically as FA-positive recipient cells [45,46].

The MTT results showed that DIL-CF-NLCs have a dose-dependent cytotoxicity. Different studies have detailed the improved cytotoxicity of drugs after being charged onto different nanocarriers [26,27], which can be credited to more effective medicate conveyance by the DDS. In this consideration, the event of apoptosis was assessed as a mechanism to eliminate the cancer cells. Examination of the cell cycle showed that DIL-CF-NLCs stopped the cancer cell by 41.2% within the Sub G1 stage at a concentration of 30 μg/mL, affirming the apoptosis in the treated cells.

The molecular docking study provides valuable insights into the potential of DIL as a modulator in targeting proteins associated with apoptosis and inflammation. With a focus on Caspase-9, which is an essential apoptosis inducer in cancer cells, the results demonstrate that DIL forms significant bonds at the active site, leading to a favorable S-score of −6.71. This suggests that DIL may effectively interact with Caspase-9, potentially inhibiting its activity and inducing apoptosis in cancer cells.

Furthermore, DIL also exhibits a binding affinity towards caspase 3 and interleukin-10, while showing a moderate interaction with interleukin-6. These findings highlight the potential of DIL as a multi-targeting agent in cancer therapy, targeting both the apoptosis and inflammation pathways. As cancer often involves the dysregulation of these processes, the ability to modulate the multiple proteins involved in these pathways could lead to improved therapeutic outcomes.

A 2016 study detailed the impacts of cell cycle arrest and apoptosis acceptance in cells treated with NLC NPs containing melatonin combined with low dosages of tamoxifen. This research showed a two-fold increment in the apoptosis rate and a 10% diminish in the cell multiplication rate [47]. Comparable outcomes were reported by Aghazadeh et al. They illustrated the pro-apoptotic impacts of kaempferol-loaded NLC-NPs by flow cytometry and molecular investigation [48]. They detailed a 22% increment in the apoptotic cells, as well as a reduction in the expression of the Bcl-2 and mcl-1genes (anti-apoptotic genes) and an increment within the expression of the Bax gene (pro-apoptotic) during treatment with kaempferol-NLCs [49]. In consideration and similar to our study, NLCs were made to provide Stylosin (STY-CFN) to MCF-7 cells through homogenization and sonication. After assessing the amount of medicate encapsulation and FA binding, the harmful impacts of STY and STY-CFN on MCF-7 cells were measured utilizing the MTT method. Cell cycle investigation, AO/PI staining, and qPCR were used to assess the apoptosis induction by STY-CFN. The results showed a significant increase in the NP size and a change in the zeta potential after coating FA-CS on the NPs. NPs with a particle size of 66.26 nm, surface charge of ±29.54 mV, and PDI of 0.3 showed a higher toxicity than STY suspension, and treatment with STY-CFN increased the number of apoptotic cells, arrested cells

in the SubG1 phase, increased the expression of caspases, and decreased the expression of Bax, BCL-2, and Bcl-xl [24]. The results of this research are similar to those of our study.

The use of combinations of routine chemotherapy, radiotherapy, and surgical methods remains valuable and is broadly utilized to treat tumors; however, the side effects are frequently a significant concern. Additionally, cancer reappearance due to an inadequate elimination of threatening cells is one of the most common reasons for a destitute prognosis [32]. Utilizing NPs for an early and precise location of cancer cells can offer assistance in dodging late conclusions, and a particular conveyance of the restricted sums of drugs straightforwardly to cancer cells can successfully diminish the side effects related to chemotherapy [33]. Simultaneously, the use of NPs may be valuable in circumventing drug resistance.

In any case, modern DDS has given a viable implication of expanding the dissolvability and steadiness of compounds, which can lead to an expanded controlled discharge, bioavailability, dissolvability, and assimilation of drugs [34]. As a new generation of lipid drug delivery systems, securing the loaded medicate and expanding its half-life, NLC increments the bioavailability and diminishes the requirement for high drug dosages [6,7]. Focusing on medication conveyance and diminishing the side effects of treatment is one of the foremost vital objectives of cancer treatments.

5. Conclusions

In common cancer treatments, side effects and drug resistance can lead to ineffectiveness, and the need for alternative therapies arises, particularly based on natural compounds. On the other hand, routine drug conveyance strategies lack efficacy for transferring medication to the target tissue, cause drug accumulation in non-target tissues, and cause side effects. In this study, DIL was chosen as a naturally active compound, and nanostructured lipid carriers were utilized after surface adjustment with chitosan-folate to extend its solvency and solidness and focused on the targeted conveyance to diverse cancer cells. The results showed an increment in treatment when utilizing this new formulation. Our results on the antioxidant, cytotoxic, pro-apoptotic, and anti-inflammatory impacts confirmed that this new approach may be promising and helpful to avoid and treat cancer, especially breast cancer. In other words, researchers should focus on validating these findings through experimental studies and optimizing the chemical structure of DIL to enhance its binding affinity and selectivity towards the targeted proteins. Ultimately, the development of a DIL-based drug with an improved efficacy and minimal side effects could provide a promising therapeutic strategy for cancer treatment.

Use of AI tools declaration

The authors declare they have not used Artificial Intelligence (AI) tools in the creation of this article.

Acknowledgments

The authors thank all colleagues at the Islamic Azad University of Tehran, and the Mashhad branch for their help and support.

Conflict of interest

All authors declare no conflicts of interest in this paper.

References

1. Jeevanandam J, Barhoum A, Chan YS, et al. (2018) Review on nanoparticles and nanostructured materials: History, sources, toxicity and regulations. *Beilstein J Nanotechnol* 9: 1050–1074. https://doi.org/10.3762/bjnano.9.98
2. Rudramurthy GR, Swamy MK (2018) Potential applications of engineered nanoparticles in medicine and biology: An update. *J Biol Inorg Chem* 23: 1185–1204. https://doi.org/10.1007/s00775-018-1600-6
3. Liu T, Bai R, Zhou H, et al. (2020) The effect of size and surface ligands of iron oxide nanoparticles on blood compatibility. *RSC Adv* 10: 7559–7569. https://doi.org/10.1039/C9RA10969B
4. Emami F, Banstola A, Vatanara A, et al. (2019) Doxorubicin and anti-PD-L1 antibody conjugated gold nanoparticles for colorectal cancer photochemotherapy. *Mol Pharmaceutics* 16: 1184–1199. https://doi.org/10.1021/acs.molpharmaceut.8b01157
5. Kiplagat A, Martin DR, Onani MO, et al. (2020) Aptamer-conjugated magnetic nanoparticles for the efficient capture of cancer biomarker proteins. *J Magn Magn Mater* 497: 166063. https://doi.org/10.1016/j.jmmm.2019.166063
6. Tagami T, Ozeki T (2017) Recent trends in clinical trials related to carrier-based drugs. *J Pharm Sci* 106: 2219–2226. https://doi.org/10.1016/j.xphs.2017.02.026
7. Varela-Fernández R, García-Otero X, Díaz-Tomé V, et al. (2022) Lactoferrin-loaded nanostructured lipid carriers (NLCs) as a new formulation for optimized ocular drug delivery. *Eur J Pharm Biopharm* 172: 144–156. https://doi.org/10.1016/j.ejpb.2022.02.010
8. Abinaya B, Prasith TP, Ashwin B, et al. (2019) Chitosan in surface modification for bone tissue engineering applications. *Biotechnology J* 14: 1900171. https://doi.org/10.1002/biot.201900171
9. Chen MC, Mi FL, Liao ZX, et al. (2013) Recent advances in chitosan-based nanoparticles for oral delivery of macromolecules. *Adv Drug Deliver Rev* 65: 865–879. https://doi.org/10.1016/j.addr.2012.10.010
10. Amini A, Kamali M, Amini B, et al. (2019) Bio-barcode technology for detection of *Staphylococcus aureus* protein A based on gold and iron nanoparticles. *Int J Biol Macromol* 124: 1256–1263. https://doi.org/10.1016/j.ijbiomac.2018.11.123
11. Zhong S, Zhang H, Liu Y, et al. (2017) Folic acid functionalized reduction-responsive magnetic chitosan nanocapsules for targeted delivery and triggered release of drugs. *Carbohyd Polym* 168: 282–289. https://doi.org/10.1016/j.carbpol.2017.03.083
12. Ruiz-Torres A, Lozano R, Melon J, et al. (2003) L-calcium channel blockade induced by diltiazem inhibits proliferation, migration and F-actin membrane rearrangements in human vascular smooth muscle cells stimulated with insulin and IGF-1. *Int J Clin Pharmacol Ther* 41: 386–391.
13. Kaddour-Djebbar I, Choudhary V, Lakshmikanthan V, et al. (2012) Diltiazem enhances the apoptotic effects of proteasome inhibitors to induce prostate cancer cell death. *J Pharmacol Exp Ther* 341: 646–655. https://doi.org/10.1124/jpet.111.188151

14. Yıldız C, Cetin A, Demirci F, et al. (2013) Anti-angiogenic effects of diltiazem, imatinib, and bevacizumab in the CAM assay. *Int J Sci Res Publ* 3: 1–8.
15. Chen YC, Wu CT, Chen JH, et al. (2022) Diltiazem inhibits breast cancer metastasis via mediating growth differentiation factor 15 and epithelial-mesenchymal transition. *Oncogenesis* 11: 48. https://doi.org/10.1038/s41389-022-00423-5
16. Li C, Wei C, Zhao G, et al. (2023) Cancer cells remodeling and quality control are inextricably linked to autophagy. *AIMS Mol Sci* 10: 109–126. https://doi.org/10.3934/molsci.2023009
17. Li P, Zhou L, Zhao T, et al. (2017) Caspase-9: Structure, mechanisms and clinical application. *Oncotarget* 8: 23996–24008. https://doi.org/10.18632/oncotarget.15098
18. Huang KH, Fang WL, Li AFY, et al. (2018) Caspase-3, a key apoptotic protein, as a prognostic marker in gastric cancer after curative surgery. *Int J Surg* 52: 258–263. https://doi.org/10.1016/j.ijsu.2018.02.055
19. Held C, White HD, Stewart RAH, et al. (2017) Inflammatory biomarkers interleukin-6 and C-reactive protein and outcomes in stable coronary heart disease: Experiences from the STABILITY (stabilization of atherosclerotic plaque by initiation of darapladib therapy) trial. *J Am Heart Assoc* 6: e005077. https://doi.org/10.1161/JAHA.116.005077
20. Iyer SS, Cheng G (2012) Role of interleukin 10 transcriptional regulation in inflammation and autoimmune disease. *Crit Rev Immunol* 32: 23–63. https://doi.org/10.1615/critrevimmunol.v32.i1.30
21. Dirican E, Özcan H, Uzunçakmak SK, et al. (2023) Evaluation expression of the caspase-3 and caspase-9 apoptotic genes in schizophrenia patients. *Clin Psychopharmacol Neurosci* 21: 171–178. https://doi.org/10.9758/cpn.2023.21.1.171
22. Vainer N, Dehlendorff C, Johansen JS (2018) Systematic literature review of IL-6 as a biomarker or treatment target in patients with gastric, bile duct, pancreatic and colorectal cancer. *Oncotarget* 9: 29820–29841. https://doi.org/10.18632/oncotarget.25661
23. Zhou L, Tang C, Li X, et al. (2022) IL-6/IL-10 mRNA expression ratio in tumor tissues predicts prognosis in gastric cancer patients without distant metastasis. *Sci Rep* 12: 19427. https://doi.org/10.1038/s41598-022-24189-3
24. Sadeghi S, Tabrizi MH, Farhadi A (2023) Folic acid-chitosan coated stylosin nanostructured lipid carriers: Fabrication, in vitro–in vivo assessment in breast malignant cells. *J Biomater Sci Polym Ed* 34: 791–809. https://doi.org/10.1080/09205063.2022.2145868
25. Al-Hasnawi HNG, Pouresmaeil V, Davoodi-Dehaghani F, et al. (2023) Synthesis folate-linked chitosan-coated quetiapine/BSA nano-carriers as the efficient targeted anti-cancer drug delivery system. *Mol Biotechnol* 1–11. https://doi.org/10.1007/s12033-023-00858-0
26. Alkwedhim MAH, Pouresmaeil V, Davoodi-Dehaghani F, et al. (2023) Synthesis and evaluation of biological effects of modified graphene oxide nanoparticles containing Lawson (Henna extract) on gastric cancer cells. *Mol Biol Rep* 50: 8971–8983. https://doi.org/10.1007/s11033-023-08797-4
27. Tuekaew J, Siriwatanametanon N, Wongkrajang Y, et al. (2014) Evaluation of the antioxidant activities of Ya-hom Intajak, a Thai herbal formulation, and its component plants. *Trop J Pharm Res* 13: 1477–1485. http://doi.org/10.4314/tjpr.v13i9.14
28. Inc CC (2016) Molecular operating environment (MOE). Chemical Computing Group Inc.
29. Chao Y, Shiozaki EN, Srinivasula SM, et al. (2005) Engineering a dimeric caspase-9: A re-evaluation of the induced proximity model for caspase activation. *PLOS Biol* 3: e183. https://doi.org/10.1371/journal.pbio.0030183

30. Ni CZ, Li C, Wu JC, et al. (2003) Conformational restrictions in the active site of unliganded human caspase-3. *J Mol Recognit* 16: 121–124. https://doi.org/10.1002/jmr.615
31. Somers W, Stahl M, Seehra JS (1997) 1.9 Å crystal structure of interleukin 6: Implications for a novel mode of receptor dimerization and signaling. *EMBO J* 16: 989–997. https://doi.org/10.1093/emboj/16.5.989
32. Yoon SI, Logsdon NJ, Sheikh F, et al. (2006) Conformational changes mediate interleukin-10 receptor 2 (IL-10R2) binding to IL-10 and assembly of the signaling complex. *J Biol Chem* 281: 35088–35096. https://doi.org/10.1074/jbc.M606791200
33. Eid RK, Ashour DS, Essa EA, et al. (2020) Chitosan coated nanostructured lipid carriers for enhanced in vivo efficacy of albendazole against *Trichinella spiralis*. *Carbohyd Polym* 232: 115826. https://doi.org/10.1016/j.carbpol.2019.115826
34. Lu B, Lv X, Le Y (2019) Chitosan-modified PLGA nanoparticles for control-released drug delivery. *Polymers* 11: 304. https://doi.org/10.3390/polym11020304
35. Liyanage PY, Hettiarachchi SD, Zhou Y, et al. (2019) Nanoparticle-mediated targeted drug delivery for breast cancer treatment. *BBA-Rev Cancer* 1871: 419–433. https://doi.org/10.1016/j.bbcan.2019.04.006
36. Rizwanullah M, Amin S, Ahmad J (2017) Improved pharmacokinetics and antihyperlipidemic efficacy of rosuvastatin-loaded nanostructured lipid carriers. *J Drug Target* 25: 58–74. https://doi.org/10.1080/1061186X.2016.1191080
37. Aibani N, Rai R, Patel P, et al. (2021) Chitosan nanoparticles at the biological interface: Implications for drug delivery. *Pharmaceutics* 13: 1686. https://doi.org/10.3390/pharmaceutics13101686
38. Danhier F, Feron O, Préat V (2010) To exploit the tumor microenvironment: Passive and active tumor targeting of nanocarriers for anti-cancer drug delivery. *J Control Release* 148: 135–146. https://doi.org/10.1016/j.jconrel.2010.08.027
39. Neves AR, Martins S, Segundo MA, et al. (2016) Nanoscale delivery of resveratrol towards enhancement of supplements and nutraceuticals. *Nutrients* 8: 131. https://doi.org/10.3390/nu8030131
40. Truong Công TTC (2012) Nanoformulations pour la protection de flavonoïdes instables: Exemple de la quercétine: Médecine humaine et pathologie. Université Paris Sud - Paris XI, 2012. Français.ffNNT: 2012PA114850ff.
41. Sou K, Inenaga S, Takeoka S, et al. (2008) Loading of curcumin in macrophages using lipid based nanoparticles. *Int J pharm* 352: 287–293. https://doi.org/10.1016/j.ijpharm.2007.10.033
42. Feliciano CP, Cammas-Marion S, Nagasaki Y (2023) Recent advances in self-assembling redox nanoparticles as a radiation protective agent. *AIMS Mol Sci* 10: 52–69. https://doi.org/10.3934/molsci.2023005
43. Padial LR, Baron-Esquivias G, Madrid AH, et al. (2016) Clinical experience with diltiazem in the treatment of cardiovascular diseases. *Cardiol Ther* 5: 75–82. https://doi.org/10.1007/s40119-016-0059-1
44. Sukhanova A, Bozrova S, Sokolov P, et al. (2018) Dependence of nanoparticle toxicity on their physical and chemical properties. *Nanoscale research letters* 13: 44. https://doi.org/10.1186/s11671-018-2457-x

45. Marshalek JP, Sheeran PS, Ingram P, et al. (2016) Intracellular delivery and ultrasonic activation of folate receptor-targeted phase-change contrast agents in breast cancer cells in vitro. *J Control Release* 243: 69–77. https://doi.org/10.1016/j.jconrel.2016.09.010
46. Monteiro CAP, Oliveira ADPR, Silva RC, et al. (2020) Evaluating internalization and recycling of folate receptors in breast cancer cells using quantum dots. *J Photochem Photobiol B* 209: 111918. https://doi.org/10.1016/j.jphotobiol.2020.111918
47. Sabzichi M, Samadi N, Mohammadian J, et al. (2016) Sustained release of melatonin: A novel approach in elevating efficacy of tamoxifen in breast cancer treatment. *Colloids and Surfaces B: Biointerfaces* 145: 64–71. https://doi.org/10.1016/j.colsurfb.2016.04.042
48. Aghazadeh T, Bakhtiari N, Rad IA, et al. (2021) Formulation of kaempferol in nanostructured lipid carriers (NLCs): a delivery platform to sensitization of MDA-MB468 breast cancer cells to paclitaxel. *Biointerface Res Appl Chem* 11: 14591–14601. https://doi.org/10.33263/BRIAC116.1459114601
49. Ni CZ, Li C, Wu JC, et al. (2003) Conformational restrictions in the active site of unliganded human caspase-3. *J Mol Recognit* 16: 121–124. https://doi.org/10.1002/jmr.615

AIMS Press